Geometry Engineering of Multiple Resonance Core via Phenyl-Embedded Strategy toward Highly Efficient Narrowband Blue OLEDs

Journal:	*Materials Horizons*
Manuscript ID	MH-COM-04-2023-000617.R1
Article Type:	Communication
Date Submitted by the Author:	21-Jun-2023
Complete List of Authors:	Wu, Yimin; Sichuan University, Liu, Xiaoyu; Sichuan University Liu, Junjie; Sichuan University Yang, Ge; Sichuan University Han, Songyan; Sichuan University, College of Chemistry Yang, Dezhi; South China University of Technology Institute of Polymer Optoelectronic Materials and Devices Cao, Xiaosong; Shenzhen University, College of Materials Sciences and Engineering Ma, Dongge; South China University of Technology, Luminescent Materials and Devices Bin, Zhengyang; Sichuan University, College of Chemistry You, Jingsong; Sichuan University, College of Chemistry

New concepts

Although multiple resonance (MR)-emitters have flourished in the recent years, blue organic light-emitting diodes (OLEDs) based on nitrogen-carbonyl-containing (N-CO) MR-emitters are still in a bottleneck situation. Many of the reported N-CO MR-emitters have limited structural diversity and typically adopt plane or [4]helicene structures, suffering from insufficient exciton utilization and unsatisfactory OLED performance. Thus, the development of advanced N-CO MR-core *via* a rational molecular engineering approach is urgently demanded yet a challenging task. Herein, we disclose a phenyl-embedded molecular design strategy to adjust the molecular curvature and achieve the improvement of N-CO MR-emitters without substituent modification. According to the geometry engineering, the introduction of bridged-phenyl ring in MR-core contributes to enhance photoluminescence quantum yield and decrease singlet-triplet energy gap simultaneously, which enables to assemble high-performance narrowband blue OLEDs with increased efficiency and reduced efficiency roll-off. This work not only provides a new avenue for the design of highly efficient MR-emitters, but also exemplifies the crucial role of molecule geometry in organic fluorophores.

Geometry Engineering of Multiple Resonance Core *via* Phenyl-Embedded Strategy toward Highly Efficient Narrowband Blue OLEDs

Received 00th January 20xx,
Accepted 00th January 20xx

DOI: 10.1039/x0xx00000x

Yimin Wu,[a] Xiaoyu Liu,[a] Junjie Liu,[a] Ge Yang,[a] Songyan Han,[a] Dezhi Yang,[b] Xiaosong Cao,[c] Dongge Ma,[b] Zhengyang Bin*[a] and Jingsong You*[a]

The geometry of molecular skeleton is of importance for the property regulation of organic electronic materials. Herein, we present a phenyl-embedded molecular design strategy to adjust the molecular curvature and achieve the improvement of blue multiple resonance (MR)-emitters. The introduction of bridged phenyl contributes to highly twisted saddle skeleton and the separation of frontier molecular orbitals, which are beneficial for the increase of photoluminescence quantum yield (PLQY) as well as the decrease of singlet-triplet energy gap (ΔE_{ST}). Consequently, *hp*-BQAO features accelerated reverse intersystem crossing rate and suppressed non-radiative decay rate simultaneously, which enables to assemble high-performance narrowband blue OLEDs with record-high external quantum efficiency (EQE) of 24.1% for the blue OLED devices exploiting nitrogen-carbonyl-containing MR-emitters without sensitizers.

Introduction

Over past decades, polycyclic heteroaromatic molecules (PHAs) have attracted immense research interest in the realm of material science due to their unique stability and tunable photophysical properties.[1] In 2019, Jiang and co-workers first employed quinolino[3,2,1-*de*]acridine-5,9-dione (**QAO**) as the thermally activated delayed fluorescence (TADF) emitter in organic light-emitting diodes (OLEDs) (Fig. 1).[2] Benefitting from the distinctive electronic effect from the oppositely positioned carbonyl groups and nitrogen atom in this rigid PHA framework, the relaxation of molecules can be restricted and the frontier molecular orbital (FMO) distributions can be well-separated, which are similar to those of the boron-nitrogen-containing (B-N) multiple resonance (MR)-emitters.[3] The OLED using the **QAO** as the emitter exhibits a maximum external quantum efficiency (EQE_{max}) of 19.4% as well as a narrow spectrum with a full-width at half-maximum (FWHM) of 39 nm. This pioneering work demonstrates the huge potential of nitrogen-carbonyl-containing (N-CO) MR-backbone for narrowband electroluminescence (EL).[4]

[a] *Key Laboratory of Green Chemistry and Technology of Ministry of Education, College of Chemistry, Sichuan University, 29 Wangjiang Road, Chengdu 610064, People's Republic of China. E-mail: binzhengyang@scu.edu.cn; jsyou@scu.edu.cn*
[b] *Institute of Polymer Optoelectronic Materials and Devices, State Key Laboratory of Luminescent Materials and Devices, South China University of Technology, Guangzhou 510640, People's Republic of China.*
[c] *Shenzhen Key Laboratory of New Information Display and Storage Materials, College of Materials Science and Engineering, Shenzhen University, Shenzhen 518060, People's Republic of China.*
Electronic Supplementary Information (ESI) available. See DOI: 10.1039/x0xx00000x

Although MR-emitters have flourished in the recent years, which cover a wide visible color, blue OLEDs based on N-CO MR-emitters are still in a bottleneck situation and the EQE values are still hovering around 20%.[2,5,6] As many of the reported N-CO MR-emitters have limited structural diversity and typically adopt plane or [4]helicene structures (Fig. 1), they are at risk of exciton quenching or excimer formation due to strong intermolecular interaction. Besides, the planar skeletons are not beneficial for the localization of FMOs distributions, which generally enlarge the singlet-triplet energy gap (ΔE_{ST}).[7] These factors lead to insufficient exciton utilization and unsatisfactory OLED performance. Although tremendous efforts have been devoted, there exist only few examples about the highly efficient blue N-CO MR-emitters up to now.[5,8] Thus, the development of advanced N-CO MR-core *via* a rational molecular engineering approach is urgently demanded yet challenging.

From the viewpoint of molecular design, the geometry of molecular skeleton is of importance for the property regulation of OLED emitters and embedding phenyl rings into PHAs judiciously would have a strong effect on the molecular geometry,[7,9] which may give a new avenue for the development of blue N-CO MR-core. Herein, we wish to disclose a phenyl-embedded molecular design strategy to adjust the molecular curvature and achieve the improvement of blue N-CO MR-emitters. In the hope of increasing the twist angle of **QAO** backbone to alleviate exciton quenching in aggregated state, we designed the phenyl-fused derivatives, **[5]*he*-BQAO** and **[6]*he*-BQAO** (Fig. 1). Furthermore, inspired by our medium-ring strategy,[10] we introduced a bridged phenyl to construct ***hp*-BQAO** containing a twisted heptagonal unit. The theoretical calculation unveils that the embedded phenyl rings alter the geometry of molecule structure as well as the distributions of FMOs while maintaining energy level. The twist angles of ***pe*-QAO**, **QAO**, **[5]*he*-BQAO**, **[6]*he*-BQAO** and ***hp*-BQAO** showcase a gradually increased tendency, which would be beneficial for the mitigation of non-radiative energy loss and the enhancement of photoluminescence quantum yield (PLQY). In particular, the FMOs of ***hp*-BQAO** are well-separated, thus potentially resulting in a small ΔE_{ST}.

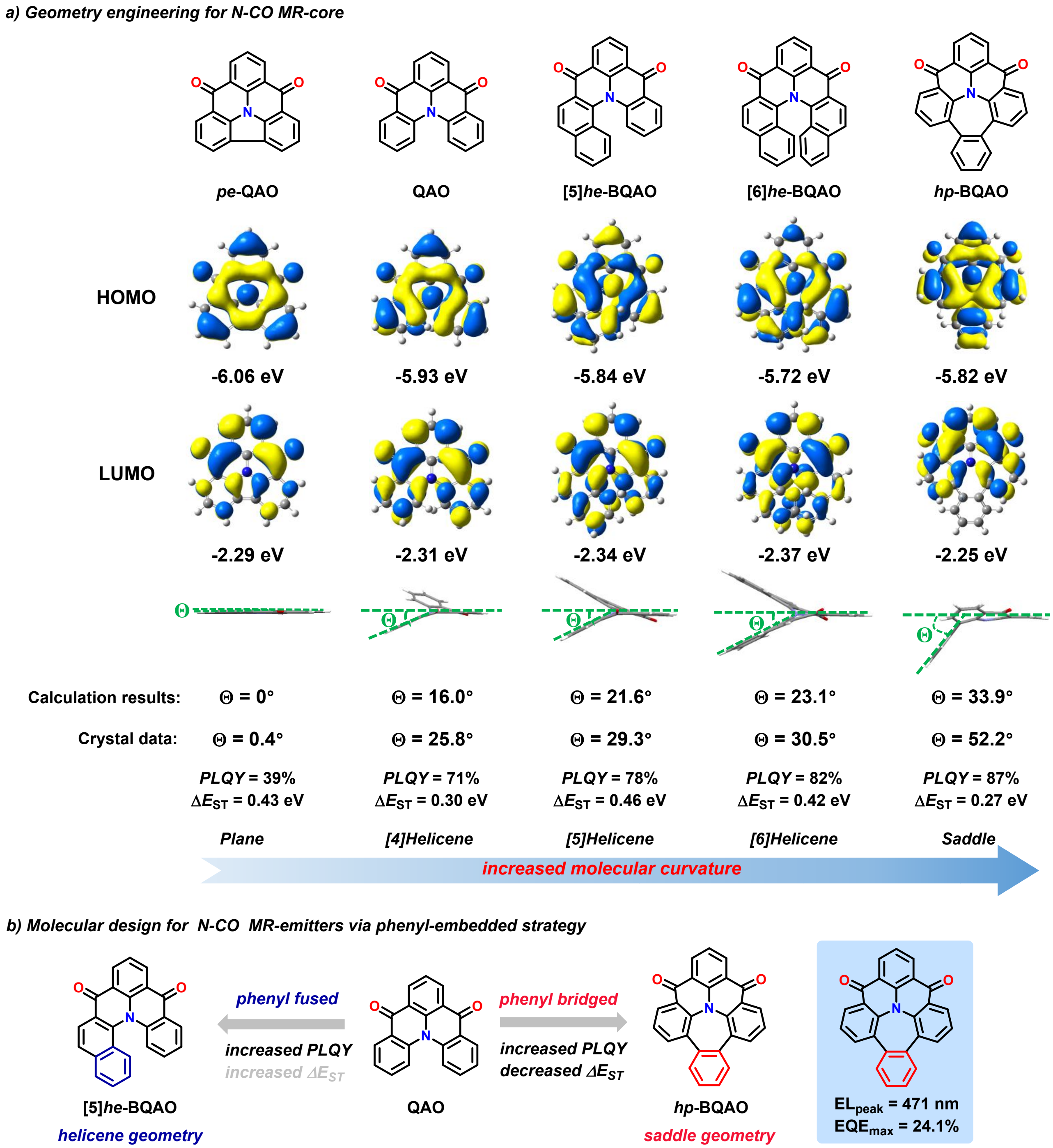

Fig. 1 Geometry engineering for N-CO MR-core.

Results and discussion

With the design strategy in hand, the synthesis of **[5]*he*-BQAO**, **[6]*he*-BQAO** and ***hp*-BQAO** was conducted and displayed in Scheme 1 and Scheme S1. For the synthesis of phenyl-fused helicene molecules, considering the large steric hindrance of the intermediates, the Buchwald–Hartwig amination reaction was a priority procedure to obtain the key precursor **3**. Then it was transformed to triarylamine derivatives *via* the Ullmann reaction and the subsequent hydrolysis and cyclization reactions smoothly furnished **[5]*he*-BQAO** and **[6]*he*-BQAO**. For the synthesis of phenyl-bridged molecule, employing the tribenzo[*b,d,f*]azepine (**9**, **TBA**) fragment as substrate, which was constructed efficiently *via* dual cross-coupling reactions including amination and direct C–H arylation,[10d] ***hp*-BQAO** was assembled rapidly. In addition, ***pe*-QAO** and **QAO** were also prepared for comparison (Scheme S2).[5b,8]

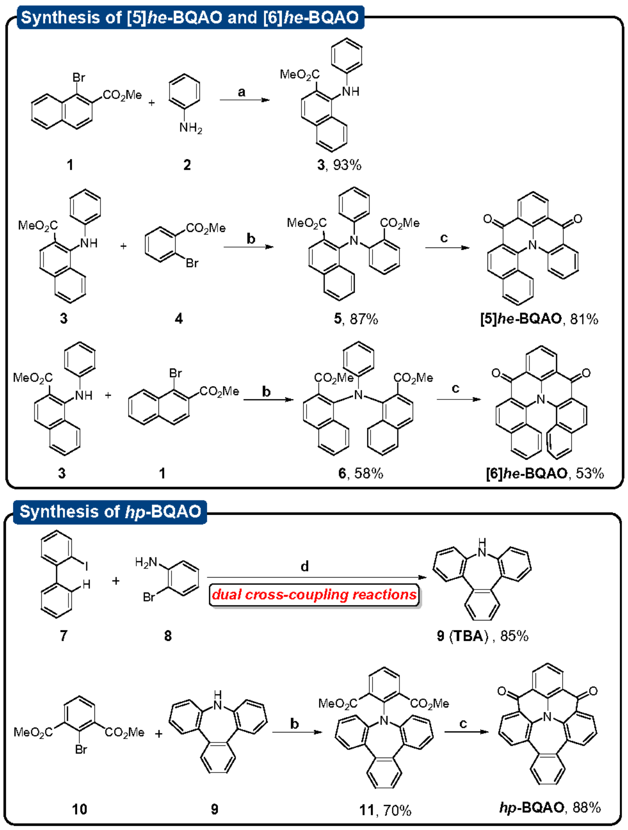

Scheme 1. Synthesis of **[5]*he*-BQAO**, **[6]*he*-BQAO** and ***hp*-BQAO**. (a) $Pd(OAc)_2$, PPh_3, Cs_2CO_3, toluene, 140 °C, 24 h; (b) Cu, K_2CO_3, *o*-DCB, 180 °C, 36 h; (c) 1) NaOH, EtOH/H_2O, 100 °C, 24 h, then 1M HCl; 2) $(COCl)_2$, cat. DMF, DCM, r.t., 1 h, then $AlCl_3$, reflux, 24 h; (d) $Pd(OAc)_2$, PPh_3, Cs_2CO_3, DMF, 120 °C, 18 h. *o*-DCB: 1,2-dichlorobenzene; DMF: *N,N*-dimethylformamide; DCM: dichloromethane.

The single crystals of ***pe*-QAO**, **QAO**, **[5]*he*-BQAO**, **[6]*he*-BQAO** and ***hp*-BQAO** were obtained though vacuum sublimation and analyzed using X-ray diffraction crystallography.[11] According to the crystal data, it is obvious that the fused phenyl increases the twist angle of the **QAO** skeleton. The crystal of ***hp*-BQAO** proves its saddle geometry and the diheral angel between the terminal phenyl ring and the center phenyl ring is 52.2°. Agreeing with the calculated results, these observations reveal that the embedded phenyl ring significantly influences the geometry of molecule structure and the saddle skeleton instead of the helicene skeleton possesses a larger twist angle. Therefore, the introduction of phenyl bridge in PHA contributes to highly twisted molecular skeleton, which could be advantageous to inhibit close packings between adjacent molecules and thus improve the performance of OLEDs.

The photophysical properties of ***pe*-QAO**, **QAO**, **[5]*he*-BQAO**, **[6]*he*-BQAO** and ***hp*-BQAO** are summarized in Fig. 2, Table 1 and Fig. S1 All the molecules display intense absorption peaks at 400-480 nm in dilute toluene solution. Attributed to its rigid planar structure and short-range charge transfer character, ***pe*-QAO** shows a sharp narrowband emission with an emission peak at 424 nm and FWHM of 14 nm. In comparison with **QAO**, **[5]*he*-BQAO**, **[6]*he*-BQAO** and ***hp*-BQAO** exhibit red-shifted emissions while maintaining narrow FWHMs (< 40 nm), which probably stem from the twisted molecular conformation that leads to spatially separated FMO distributions and enhanced charge-transfer character. To investigate the intramolecular charge-transfer properties of these compounds, the fluorescence spectra were further measured in differently polar solvents (Fig. S2 and Table S7). With the increased polarity of solvents, ***hp*-BQAO** exhibits more significantly red-shifted emissions with broadened character than **QAO**, indicative of the enhanced charge-transfer property. According to the phosphorescence spectra measured at 77 K, **[5]*he*-BQAO** and **[6]*he*-BQAO** possess lower triplet state energy than other molecules due to the naphthalene fused in the PHA. As a result, the ΔE_{ST} values were determined to be 0.43 eV, 0.30 eV, 0.46 eV, 0.42 eV and 0.27 eV for ***pe*-QAO**, **QAO**, **[5]*he*-BQAO**, **[6]*he*-BQAO** and ***hp*-BQAO**, respectively. As these data demonstrate, the phenyl-bridged derivatives with a more twisted structure have a reduction of ΔE_{ST} compared with **QAO**.

Table 1. Summary of photophysical and thermal data

Compound	λ_{abs}[a] [nm]	λ_{em}[b] [nm]	FWHM[b] [nm]	E_{S1} [eV]	E_{T1} [eV]	ΔE_{ST} [eV]	Φ_{PL}[c] [%]	τ_p[c] [ns]	τ_d[c] [μs]	C_1[d] [%]	C_2[e] [%]	k_R^S[f] [10^7 s^{-1}]	k_{NR}^T[g] [10^4 s^{-1}]	k_{RISC}[h] [10^5 s^{-1}]	T_g[g] [℃]
***pe*-QAO**	418	424/466	13/79	3.04	2.61	0.43	39	0.5	-	-	-	-	-	-	363
QAO	434	452/466	25/36	2.88	2.58	0.30	71	7.3	4.8	78.2	21.8	7.6	13.5	1.3	275
[5]*he*-BQAO	438	458/477	32/40	2.88	2.42	0.46	78	2.3	-	-	-	-	-	-	280
[6]*he*-BQAO	452	474/494	34/44	2.76	2.34	0.42	82	2.8	-	-	-	-	-	-	-
***hp*-BQAO**	436	456/473	34/42	2.87	2.60	0.27	87	3.6	13.4	28.0	72.0	6.8	1.3	2.5	410

[a] Measured in toluene solution (1.0×10^{-5} M) at 298 K. [b] Measured in toluene solution (1.0×10^{-5} M)/ in 3 wt% DCz-BTP host-blended film at 298 K. [c] Measured in 3 wt% DCz-BTP host-blended film at 298 K. Proportion of [d] prompt (C_1) and [e] delayed (C_2) components. [f] $k_R^S = C_1\Phi_{PL}/\tau_p$. [g] $k_{NR}^T = (1-\Phi_{PL})/[\tau_d(1-\Phi_{PL}C_1)]$. [h] $k_{RISC} = C_2/[C_1\tau_d(1-\Phi_{PL}C_1)]$. [g] Decomposition temperatures corresponding to 5% weight loss.

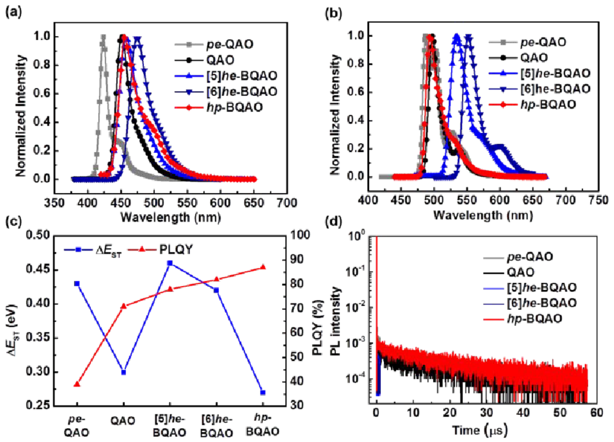

Fig. 2 (a) Fluorescence (Fl.) spectra at 298 K and (b) phosphorescence (Phos.) spectra at 77 K in toluene solutions at 1.0 × 10^{-5} M. (c) ΔE_{ST} calculated based on Fl. and Phos. spectra in toluene solutions at 1.0 × 10^{-5} M and PLQYs of the 3 wt% **DCz-BTP** host-blended films. (d) Transient PL spectra of the 3 wt% **DCz-BTP** host-blended films at 298 K.

Moreover, the photophysical properties were further evaluated in the 3,6-di(9*H*-carbazol-9-yl)benzo[4,5]thieno[2,3-*b*]pyridine (**DCz-BTP**) host-blended films at 3 wt%.[12] According to the transient photoluminescence spectra (Fig. 2d), ***hp*-BQAO** exhibits prompt lifetimes (τ_p) of 3.6 ns as well as delayed lifetimes (τ_d) of 13.4 μs, respectively, ensuring its TADF properties. In comparison with **QAO**, ***hp*-BQAO** possesses a smaller ΔE_{ST} but a longer τ_d, which is probably attributed to the less affected triplet states of the twisted MR-emitters by the surroundings.[13] As for ***pe*-QAO**, **[5]*he*-BQAO** and **[6]*he*-BQAO** that possess large ΔE_{ST}, only short-lived prompt fluorescence was observed, indicating the absence of TADF nature. In addition, the ***pe*-QAO**-doped film reveals a broadband spectrum (FWHM = 79 nm) with a low PLQY of 39% because of its planar configuration. Meanwhile, the phenyl-fused and phenyl-bridged derivatives both showcase an improvement of PLQY for the reference **QAO**, and ***hp*-BQAO**-doped film gives an outstanding PLQY of 87%. These results not only disclose that increasing the twist angles of the PHA skeletons could contribute to the separation of FMOs, so as to decrease ΔE_{ST} value, but also uncover the crucial role of the molecular curvature for the development of **QAO**-based emitters with high PLQY. Furthermore, to investigate the aggregation phenomenon of the phenyl-fused and phenyl-bridged derivatives in solid state, the doped films of **[5]*he*-BQAO**, **[6]*he*-BQAO** and ***hp*-BQAO** were prepared with doping concentrations of 1 wt%, 3 wt%, 5 wt%, 10 wt% and 20 wt% in **DCz-BTP** (Fig. S3). As the doping concentration increased, the emission spectra of phenyl-fused derivatives-doped films are significantly broadened with drastically decreased PLQY values ($PLQY_{3\%}$ = 78% and $PLQY_{20\%}$ = 48% for **[5]*he*-BQAO**; $PLQY_{3\%}$ = 82% and $PLQY_{20\%}$ = 61% for **[6]*he*-BQAO**). Due to its highly twisted molecular structure, the aggregation-caused quenching (ACQ) effect of ***hp*-BQAO** is inhibited ($PLQY_{3\%}$ = 87% and $PLQY_{20\%}$ = 79%) and the spectrum broadening is suppressed. As summarized in Table 1, the reverse intersystem crossing rate (k_{RISC}) of ***hp*-BQAO** was calculated to be 2.5 × 10^5 s^{-1}, which are faster than that of **QAO** (1.3 × 10^5 s^{-1}) due to smaller ΔE_{ST}. Besides, according to spin-orbit coupling (SOC) analysis, ***hp*-BQAO** with a dense manifold of triplet states possesses more efficient RISC channels than **QAO**, so as to increase k_{RISC} (Fig. S4). Notably, the triplet non-radiative decay rate (k_{NR}^{T}) of ***hp*-BQAO** (1.3 × 10^4 s^{-1}) was tenfold slower than that of **QAO** (1.4 × 10^5 s^{-1}), proving the rigid twisted molecular structure is favourable to constrict the non-radiative decay, so as to improve the PLQY of MR-emitters without substituent modification.

Finally, to evaluate their EL performances, blue OLEDs were assembled using ***pe*-QAO**, **QAO**, **[5]*he*-BQAO** and ***hp*-BQAO** as the emitters and **DCz-BTP** as the host. Considering its blue-greenish emission in solid state and relatively large ΔE_{ST}, **[6]*he*-BQAO** is not discussed here. Prior to OLED fabrication, the thermogravimetric analysis was conducted, which reveals the good thermal stability of these compounds (Fig. S5). The optimized device structure is ITO/1,1-bis[(di-4-tolylamino)phenyl] cyclohexane (**TAPC**, 30 nm)/tris(4-carbazolyl-9-ylphenyl)amine (**TCTA**, 10 nm)/EMLs (20 nm)/1,3,5-tri[(3-pyridyl)-phen-3-yl]benzene (**TmPyPb**, 45 nm)/LiF (0.8 nm)/Al (100 nm) (Fig. 3a and 3b). Similar to **QAO**, the phenyl-fused and phenyl-bridged derivatives both feature narrowband EL emission peaks around 470 nm at the doping concentration of 3 wt% (Fig. 3c). Remarkably high EQE_{max} of 24.1% was observed for devices with ***hp*-BQAO**, as revealed in Fig. 3d and Table 2, representing one of the best results for blue OLED devices exploiting N-CO MR-emitters without sensitizers (Fig. 3e and Table S8).[4] Meanwhile, the ***hp*-BQAO**-based OLEDs display reduced efficiency roll-off in comparison with **QAO**. Moreover, ***hp*-BQAO**-based OLEDs also exhibit better operation stability than **QAO**-based OLEDs (Fig. S6). The state-of-the-art performances testify the great potential of rigid twisted ***hp*-BQAO** core, which manifests faster reverse intersystem crossing rate, slower non-radiative decay rate and larger horizontal orientation factors (Fig. S7). The larger ΔE_{ST} of **[5]*he*-BQAO** results in a low EQE_{max} of 3.3% for the **[5]*he*-BQAO**-based OLEDs. Owing to its planar conformation inducing strong intermolecular interactions with the surroundings, the device with ***pe*-QAO** showcases a broad EL spectrum (FWHM = 75 nm) with an EQE above 5%.[8]

Table 2. Summary of OLED performances

Emitter	V_{on}^{a} [V]	EL_{peak}^{b} [nm]	FWHM^{c} [nm]	PE_{max}^{d} [lm/W]	$EQE_{max/100/1000}^{e}$ [%]
***pe*-QAO**	3.1	468	75	12.4	9.0/6.0/1.2
QAO	3.1	465	36	19.1	17.7/11.1/3.7
[5]*he*-BQAO	3.3	471	43	4.9	3.3/1.6/1.2
***hp*-BQAO**	3.0	471	41	33.0	24.1/18.1/8.2

^{a} Turn-on voltage at at 1 cd m^{-2}. ^{b} EL emission peak at 1000 cd m^{-2}. ^{c} full-width at half-maximum. ^{d} Power efficiency. ^{e} External quantum efficiency.

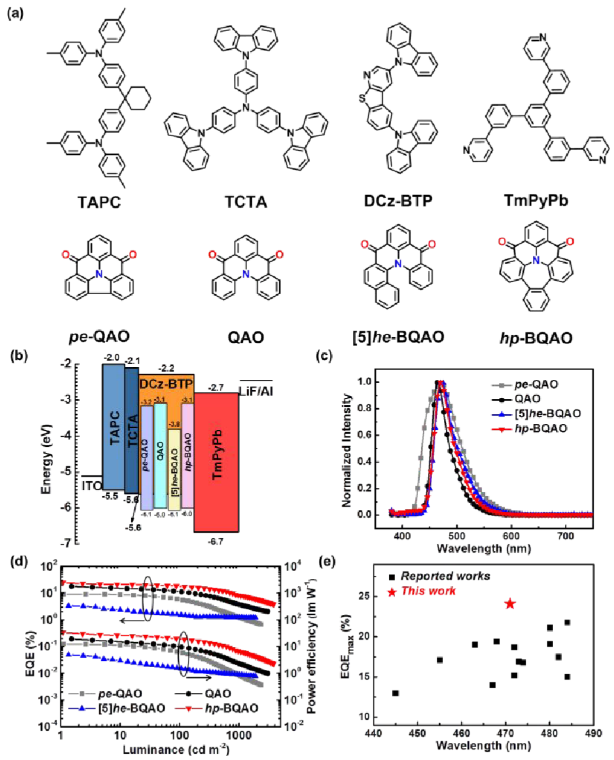

Fig. 3 (a) Molecular structures used in OLEDs. (b) OLEDs structure with corresponding energy levels. (c) EL spectra measured at 1000 cd m^{-2}. (d) EQE-luminance-power efficiency curves of OLEDs. (e) EL$_{peak}$ and EQE$_{max}$ summary of blue OLEDs exploiting N-CO MR-emitters without sensitizers (For the detailed data, see Table S8).

Conclusions

In conclusion, we have put forward a feasible phenyl-embedded molecular design strategy to adjust the molecular curvature and realize the improved efficiency of blue N-CO MR-emitters without substituent modification. The embedded phenyl ring gives rise to the twist angle of molecule structure to retard exciton quenching in aggregated state, so as to promote the PLQY. Besides, the phenyl-bridged derivatives feature the twisted saddle skeleton, leading to the increase of PLQY and the decrease of ΔE_{ST} simultaneously. Consequently, the blue emitter ***hp*-BQAO** possessing accelerated reverse intersystem crossing rate and suppressed non-radiative decay rate enables superior EL performance with an EQE up to 24.1% while maintaining a narrowband emission, which indicates the importance of molecular geometry for the designing of high-performance organic fluorophores. Further optimization about molecule derivation and device engineering is currently in progress in our lab.

Conflicts of interest

There are no conflicts to declare.

Acknowledgements

We acknowledge financial support from the National NSF of China (Nos 22031007, 22275127 and 22005204).

Notes and references

1 (*a*) M. Stępień, E. Gońka, M. Żyła and N. Sprutta, *Chem. Rev.* 2017, **117**, 3479-3761; (*b*) A. Borissov, Y. K. Maurya, L. Moshniaha, W.-S. Wong, M. Żyła-Karwowska and M. Stępień, *Chem. Rev.* 2022, **122**, 565-788.

2 Y. Yuan, X. Tang, X.-Y. Du, Y. Hu, Y.-J. Yu, Z.-Q. Jiang, L.-S. Liao and S.-T. Lee. *Adv. Optical Mater.* 2019, **7**, 1801536.

3 (*a*) T. Hatakeyama, K. Shiren, K. Nakajima, S. Nomura, S. Nakatsuka, K. Kinoshita, J. Ni, Y. Ono and T. Ikuta, *Adv. Mater*. 2016, **28**, 2777-2781; (*b*) H. Jiang, Y. Cao, Q. Yang, L. Xian, Y. Tao, R. Chen and W. Huang, *J. Phys. Chem. Lett*. 2020, **11**, 7739-7754; (*c*) S. Madayanad Suresh, D. Hall, D. Beljonne, Y. Olivier and E. Zysman-Colman, *Adv. Funct. Mater.* 2020, **30**, 1908677.

4 (*a*) J.-M. Teng, Y.-F. Wang and C.-F. Chen, *J. Mater. Chem. C*. 2020, **8**, 11340-11353; (*b*) J. M. Ha, S. H. Hur, A. Pathak, J.-E. Jeong and H. Y. Woo, *NPG Asia Materials* 2021, **13**, 53-88; (*c*) G. Hong, X. Gan, C. Leonhardt, Z. Zhang, J. Seibert, J. M. Busch and S. Bräse, *Adv. Mater.* 2021, **33**, 2005630; (*d*) H. J. Kim and T. Yasuda, *Adv. Optical Mater.* 2022, **10**, 2201714; (*e*) Y.-J. Yu, F.-M. Liu, X.-Y. Meng, L.-Y. Ding, L.-S. Liao and Z.-Q. Jiang, *Chem. Eur. J.* 2022, **29**, e202202628.

5 (*a*) X. Li, Y.-Z. Shi, K. Wang, M. Zhang, C.-J. Zheng, D.-M. Sun, G.-L. Dai, X.-C. Fan, D.-Q. Wang, W. Liu, Y.-Q. Li, J. Yu, X.-M. Ou, C. Adachi and X.-H. Zhang, *ACS Appl. Mater. Interfaces* 2019, **11**, 13472-13480; (*b*) D. Hall, S. M. Suresh, P. L. dos Santos, E. Duda, S. Bagnich, A. Pershin, P. Rajamalli, D. B. Cordes, A. M. Z. Slawin, D. Beljonne, A. Köhler, I. D. W. Samuel, Y. Olivier and E. Zysman-Colman, *Adv. Optical Mater.* 2020, **8**, 1901627; (*c*) X. Qiu, G. Tian, C. Lin, Y. Pan, X. Ye, B. Wang, D. Ma, D. Hu, Y. Luo, Y. Ma, *Adv. Optical Mater.* 2021, **9**, 2001845; (*d*) S.-Y. Yang, S.-N. Zou, F.-C. Kong, X.-J. Liao, Y.-K. Qu, Z.-Q. Feng, Y.-X. Zheng, Z.-Q. Jiang and L.-S. Liao, *Chem. Commun.* 2021, **57**, 11041-11044; (*e*) S.-N. Zou, C.-C. Peng, S.-Y.Yang, Y.-K. Qu, Y.-J. Yu, X. Chen, Z.-Q. Jiang and L.-S. Liao, *Org. Lett.* 2021, **23**, 958-962; (*f*) Y.-J. Yu, S.-N. Zou, C.-C. Peng, Z.-Q. Feng, Y.-K. Qu, S.-Y. Yang, Z.-Q. Jiang and L.-S. Liao, *J. Mater. Chem. C* 2022, **10**, 4941-4946; (*g*) S. Wu, A. K. Gupta, K. Yoshida, J. Gong, D. Hall, D. B. Cordes, A. M. Z. Slawin, I. D. W. Samuel and E. Zysman-Colman, *Angew. Chem. Int. Ed.* 2022, **61**, e202213697.

6 H. Min, I. S. Park and T. Yasuda, *Angew. Chem. Int. Ed.* 2021, **60**, 7643-7648.

7 Y. Shi, G. Yang, B. Shen, Y. Yang, L. Yan, F. Yang, J. Liu, X. Liao, P. Yu, Z. Bin and J. You, *J. Am. Chem. Soc.* 2021, **143**, 21066-21076.

8 C. Cao, J.-H. Tan, Z.-L. Zhu, J.-D. Lin, H.-J. Tan, H. Chen, Y. Yuan, M.-K. Tse, W.-C. Chen and C.-S. Lee, *Angew. Chem. Int. Ed.* 2023, **62**, e202215226.

9 (*a*) M. Hirai, N. Tanaka, M. Sakai and S. Yamaguchi, *Chem. Rev.* 2019, **119**, 8291-8331; (*b*) J. M. dos Santos, D. Sun, J. M. Moreno-Naranjo, D. Hall, F. Zinna, S. T. J. Ryan, W. Shi, T. Matulaitis, D. B. Cordes, A. M. Z. Slawin, D. Beljonne, S. L. Warriner, Y. Olivier, M. J. Fuchter and E. Zysman-Colman, *J. Mater. Chem. C* 2022, **10**, 4861-4870; (*c*) J. Wagner, P. Z. Crocomo, M. A. Kochman, A. Kubas, P. Data and M.Lindner, *Angew. Chem. Int. Ed.* 2022, **61**, e202202232.

10 (*a*) Z. Huang, Z. Bin, R. Su, F. Yang, J. Lan and J. You, *Angew. Chem. Int. Ed.* 2020, **59**, 9992-9996; (*b*) W. Ma, Z. Bin, G. Yang, J. Liu and J. You, *Angew. Chem. Int. Ed.* 2022, **61**, e202116681; (*c*) Z. Huang, B. Lei, D. Yang, D. Ma, Z. Bin and J.

You, *Angew. Chem. Int. Ed.* 2022, **61**, e202213157; (*d*) B. Lei, Z. Huang, S. Li, J. Liu, Z. Bin and J. You, *Angew. Chem. Int. Ed.* 2023, **62**, e202218405.

11 CCDC 2249621 (**6**), CCDC 2249111 (***pe*-QAO**), CCDC 2248788 (**QAO**), CCDC 2248789 (**[5]*he*-BQAO**), CCDC 2248790 (**[6]*he*-BQAO**) and CCDC 2249112 (***hp*-BQAO**) contain the supplementary crystallographic data for this paper.

12 F. Wang, L. Zhang, W. Han, Z. Bin and J. You, *Angew. Chem. Int. Ed.* 2022, **61**, e202205380.

13 (*a*) Y. Zhang, J. Wei, D. Zhang, C. Yin, G. Li, Z. Liu, X. Jia, J. Qiao and L. Duan, *Angew. Chem. Int. Ed.* 2022, **61**, e202113206; (*b*) D. Zhang, Y. Wada, Q. Wang, H. Dai, T. Fan, G. Meng, J. Wei, Y. Zhang, K. Suzuki, G. Li, L. Duan and H. Kaji, *Adv. Sci.* 2022*,* **9***,* 2106018; (*c*) W. Yang, J. Miao, F. Hu, Y. Zou, C. Zhong, S. Gong and C. Yang, *Adv. Funct. Mater.* 2023*,* **33***,* 2213056; (*d*) Y. Hu, J. Miao, C. Zhong, Y. Zeng, S. Gong, X. Cao, X. Zhou, Y. Gu and C. Yang, *Angew. Chem. Int. Ed.* 2023, **62**, e202302478.

